Filament Depolymerization Can Explain Chromosome Pulling during Bacterial Mitosis

Edward J. Banigan[1], Michael A. Gelbart[2,3], Zemer Gitai[4], Ned S. Wingreen[4]*, Andrea J. Liu[1]*

1 Department of Physics and Astronomy, University of Pennsylvania, Philadelphia, Pennsylvania, United States of America, **2** Graduate Program in Biophysics, Harvard University, Boston, Massachusetts, United States of America, **3** Department of Physics, Princeton University, Princeton, New Jersey, United States of America, **4** Department of Molecular Biology, Princeton University, Princeton, New Jersey, United States of America

Abstract

Chromosome segregation is fundamental to all cells, but the force-generating mechanisms underlying chromosome translocation in bacteria remain mysterious. *Caulobacter crescentus* utilizes a depolymerization-driven process in which a ParA protein structure elongates from the new cell pole, binds to a ParB-decorated chromosome, and then retracts via disassembly, pulling the chromosome across the cell. This poses the question of how a depolymerizing structure can robustly pull the chromosome that disassembles it. We perform Brownian dynamics simulations with a simple, physically consistent model of the ParABS system. The simulations suggest that the mechanism of translocation is "self-diffusiophoretic": by disassembling ParA, ParB generates a ParA concentration gradient so that the ParA concentration is higher in front of the chromosome than behind it. Since the chromosome is attracted to ParA via ParB, it moves up the ParA gradient and across the cell. We find that translocation is most robust when ParB binds side-on to ParA filaments. In this case, robust translocation occurs over a wide parameter range and is controlled by a single dimensionless quantity: the product of the rate of ParA disassembly and a characteristic relaxation time of the chromosome. This time scale measures the time it takes for the chromosome to recover its average shape after it is has been pulled. Our results suggest explanations for observed phenomena such as segregation failure, filament-length-dependent translocation velocity, and chromosomal compaction.

Citation: Banigan EJ, Gelbart MA, Gitai Z, Wingreen NS, Liu AJ (2011) Filament Depolymerization Can Explain Chromosome Pulling during Bacterial Mitosis. PLoS Comput Biol 7(9): e1002145. doi:10.1371/journal.pcbi.1002145

Editor: Dennis R. Livesay, UNC Charlotte, United States of America

Received April 23, 2011; **Accepted** June 20, 2011; **Published** September 22, 2011

Funding: We gratefully acknowledge the support of the NSF (http://www.nsf.gov) through DMR-0605044 (EJB and AJL), DMR-0520020 (AJL), and PHY-0957573 (NSW). ZG is supported by a HFSP (http://www.hfsp.org/) Young Investigator Award and NIH (http://www.nih.gov/) grant 1DP2OD004389. The funders had no role in study design, data collection and analysis, decision to publish, or preparation of the manuscript.

Competing Interests: The authors have declared that no competing interests exist.

* E-mail: ajliu@physics.upenn.edu (AJL); wingreen@princeton.edu (NSW)

Introduction

Several processes involved in DNA partitioning rely on depolymerization of filaments for translocation. In eukaryotes, depolymerizing microtubules [1] position chromosomes before cell division via macromolecular couplers and/or molecular motors bound to the microtubules [2,3]. In prokaryotes, however, no such coupler or motor has been identified. Instead, proteins bound to the chromosome or plasmid bind directly to filaments and trigger their depolymerization [4,5]. This poses the question of whether in the absence of a coupler, DNA can be pulled in a robust fashion, without becoming detached from the filaments as they disassemble.

Type I low-copy-number-plasmids [6,7], chromosome I of *Vibrio cholerae* [8], and the chromosome of *Caulobacter crescentus* [9–12] all share a common segregation mechanism that relies on pulling mediated by filament depolymerization. This conserved system relies on three central components: the ATPase ParA, the DNA-binding protein ParB, and a centromere-like DNA locus. ParA is a deviant Walker-type ATPase that upon binding ATP forms dimers that can polymerize and associate with DNA [10,13]. ParB interacts with ParA directly and stimulates ATP hydrolysis, causing ParA to dissociate into free monomers [13]. The spatial and temporal organization of ParA and the ParB-binding *parS* chromosomal locus can lead to robust chromosome segregation *in vivo*. For example, in *C. crescentus*, the chromosomal origin (*ori*) is initially localized at a single cell pole (the "stalked" pole) [14], and must translocate to the opposite "swarmer" pole before cell division. In predivisional cells, approximately one thousand ParB are bound via *parS* near the origin of the chromosome (*ori*) [9,15]. There appear to be several distinct stages of ParB-*parS*-*ori* complex translocation [11]; our focus is on the final, most rapid stage in which the complex binds to filaments of ParA and translates from partway across the cell to the swarmer pole at a velocity of $v \approx 0.3\ \mu\mathrm{m/min}$ [9,11,16,17]. As the ParA bundle depolymerizes, presumably due to ParB-induced ATP hydrolysis or nucleotide exchange [7–11,13,15,18,19], the ParB-*parS*-*ori* complex remains localized near the edge of the ParA structure [8,10–12].

For eukaryotic chromosome segregation driven by depolymerization of microtubules [2,3], models generally assume the existence of a "coupler" that attaches the chromosome to the depolymerizing microtubules. This coupler moves along the microtubule ahead of the depolymerizing end, either because it slides along it diffusively [20–24], because it is pushed by conformational changes near the tip of the microtubule [23–26], or because it has a complex internal structure that causes it to process [3,27]. Of the existing models of bacterial chromosome segregation [28–33], only a few address the question of how depolymerizing proteins can cause translocation. Typically, these

Author Summary

Reliable chromosome segregation is crucial to all dividing cells. In some bacteria, segregation has been found to occur in a rather counterintuitive way: the chromosome attaches to a filament bundle and erodes it by causing depolymerization of the filaments. Moreover, unlike eukaryotic cells, bacteria do not use molecular motors and/or macromolecular tethers to position their chromosomes. This raises the general question of how depolymerizing filaments alone can continuously and robustly pull cargo as the filaments themselves are falling apart. In this work, we introduce the first quantitative physical model for depolymerization-driven translocation in a many-filament system. Our simulations of this model suggest a novel underlying mechanism for robust translocation, namely self-diffusiophoresis, motion of an object in a self-generated concentration gradient in a viscous environment. In this case, the cargo generates and sustains a concentration gradient of filaments by inducing them to depolymerize. We demonstrate that our model agrees well with existing experimental observations such as segregation failure, filament-length-dependent translocation velocity, and chromosomal compaction. In addition, we make several predictions–including predictions for the specific modes by which the chromosome binds to the filament structure and triggers its disassembly–that can be tested experimentally.

models attempt to explain ParAB partitioning systems with reaction-diffusion models or general thermodynamic arguments, but do not address the conditions required for robust translocation [31,32].

Here we ask whether depolymerization of ParA by ParB without a coupler is sufficient to explain the observed translocation in prokaryotic DNA partitioning. We performed Brownian dynamics simulations that explicitly incorporate the biochemistry of the primary constituents of the ParABS segregation system. In our simulations, a polymer representing the ParB-*parS*-*ori* complex (henceforth referred to as the "ParB polymer"), binds to a filamentous ParA bundle and initiates disassembly of ParA. We find that the ParB polymer can indeed exhibit robust, depolymerization-driven translocation via a novel mechanism (Fig. 1), provided certain conditions are met.

Results

Simulating ParB translocation

To understand the mechanism by which ParA translocates ParB, we performed Brownian dynamics simulations of a ParB polymer interacting with an anchored ParA filament bundle (Fig. 1c). The ParB polymer, shown in Figs. 1b–c, corresponds to the ParB-*parS*-*ori* complex. It is represented by a semi-flexible chain of monomeric subunits, typically of length 100 subunits. The center section (dark green in Fig. 1b), typically of length 50 subunits, represents the part of the chromosome that binds to ParA via ParB, while the two peripheral segments (light green in Fig. 1b only) cannot bind to ParA.

During robust translocation, the ParB polymer remains localized near the tip of the ParA bundle and moves across the cell (see snapshots in Fig. 1c and Video S1). By inducing disassembly, ParB creates a concentration gradient of ParA filaments that remains fixed with respect to the center of mass of the ParB polymer. Thus, the ParA concentration profile

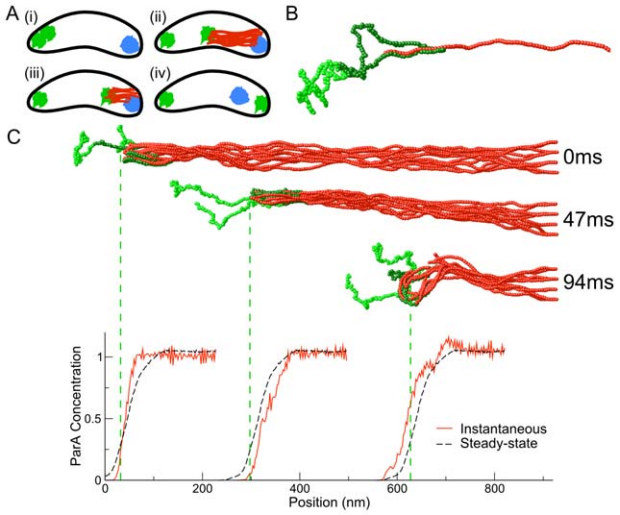

Figure 1. Schematic model for chromosome segregation and simulation snapshots. (A) Model of chromosome segregation in *Caulobacter crescentus*. (*i*) Initially, the two copies of the origin of replication (*ori* - green) and the terminus (*ter* - blue) of the chromosome are localized at the stalked and swarmer poles, respectively. (*ii*) The two origins separate and a structure of ParA protein (red) emanating from the swarmer pole comes into contact with the medial origin; ParB, polymerized on the chromosome near the origin, binds to ParA. (*iii*) ParB and the origin localize with the end of the ParA and move across the cell as ParA depolymerizes. (*iv*) The origin localizes near the swarmer pole; the terminus moves towards mid-cell. (B) Snapshot of ParB-ParA binding in simulation. The central strip of the ParB polymer (dark green) binds side-on to ParA filaments, whereas the peripheral segments of the ParB polymer (light green) cannot bind to ParA. (C) Snapshots of the full simulation and corresponding ParA filament concentration profiles (red). The dashed green lines indicate the center of mass of the ParB polymer. ParB binds to ParA and disassembles the ParA bundle (for clarity, depolymerized ParA monomers are not displayed). This interaction creates a steady-state ParA filament concentration gradient (black), which moves with and transports the ParB across the cell, providing a mechanism for chromosome segregation.
doi:10.1371/journal.pcbi.1002145.g001

translocates with the ParB, and exhibits only small, short-lived fluctuations around a well-defined steady-state mean (Fig. 1c).

Translocation is most robust when ParB binds side-on to ParA

Since the precise nature of the ParB–ParA interaction is unknown, we used our simulations to identify the modes of binding and disassembly that provide robust translocation. In our model (see Methods), ParB binds to ParA subunits in the filament bundle (Fig. 1c). The ParB polymer hydrolyzes ParA subunits that it binds to; once a subunit at the tip of a ParA filament is hydrolyzed, it can depolymerize from the filament. Monomers rapidly diffuse away once they have depolymerized. Some interaction/disassembly mechanisms or parameter ranges lead to robust translocation of the ParB polymer, while others lead to failure by rapid detachment:

Tip-only binding. In this model, ParB binds only to the tips of ParA filaments (Fig. 2a). Since the number of ParA filament tips is limited, the ParB polymer is held only weakly to the ParA bundle, and small fluctuations can cause it to detach (Fig. 2a). In principle, this failure mode could be suppressed by increasing the number of ParA filaments within the bundle, but translocation is intrinsically fragile for this model.

Side-binding with filament severing. As an alternative, we allow ParB to bind to the sides of the ParA filaments (Fig. 1b). In this

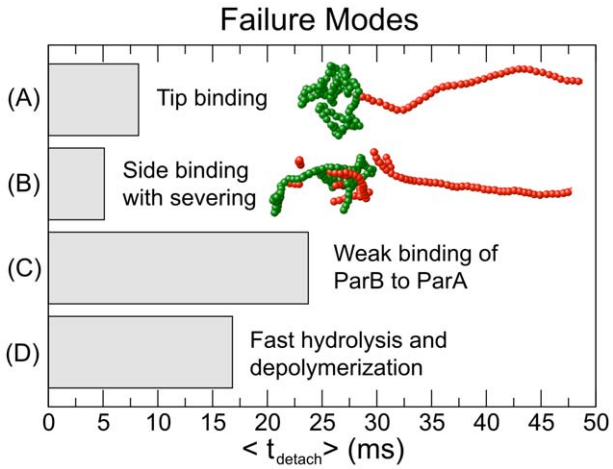

Figure 2. Mean time, $\langle t_{\mathrm{detach}} \rangle$, to first detachment of ParB polymer from ParA for various failure modes. In a standard simulation, ParB binds ParA filaments side-on, and hydrolyzes individual ParA subunits. Hydrolyzed ParA disassembles from the tip of each filament in the bundle. In a typical simulation it takes about 200ms for the ParB polymer to translocate across a distance of 1 μm. However, ParB completely detaches in a short time if (A) the ParB polymer binds to only the tips of the ParA filaments or (B) if ParA filaments disassemble via mid-filament severing. In addition, the ParB polymer detaches if (C) ParB binds too weakly to ParA or (D) ParA disassembles too quickly. Measurements for (A) and (B) are taken from simulations with side-binding with severing or tip binding, respectively, with standard parameters. Measurements for (C) and (D) are taken from simulations with the slowest disassembly rate or highest binding energy, respectively, for which the mean time to first detachment is shorter than the time required for the ParB polymer to translocate across the cell.
doi:10.1371/journal.pcbi.1002145.g002

model, ParA filaments can disassemble by severing in addition to disassembling from the filament tips (Fig. 2b). Severing may occur at the location of any ParA subunit that has been hydrolyzed by ParB. Typically, we find that the ParB polymer binds to multiple severed ParA segments, preventing ParB from binding to the remaining filaments in the ParA bundle (Video S2). As a result, the ParB polymer rapidly detaches from the anchored bundle. ParA severing therefore does not lead to reliable ParB translocation.

Side-binding with tip-only disassembly. In this model, ParB binds side-on to ParA filaments (Figs. 1b–c) and ParA disassembles only at the filament tips. In this case, the ParB polymer translocates across the cell without detaching from the ParA bundle for a wide range of parameters. However, under certain extreme conditions, translocation fails:

Weak binding. If the ParB–ParA binding energy, ϵ, is too small, ParB quickly detaches from ParA due to thermal noise and the force from the rest of the ParB polymer (Fig. 2c).

Fast hydrolysis and depolymerization. Rapid detachment occurs if the ParA hydrolysis rate, k_h, and ParA depolymerization rate, k_d, are both too large (Fig. 2d).

Our major result is that translocation is most robust in the side-binding model with disassembly only from the tips of ParA filaments. The rest of our simulations use this robust mode of disassembly and translocation, and henceforth, we refer to side-binding with tip-only disassembly as our standard model.

The rate of disassembly controls the ParB translocation velocity

To understand how ParA translocates ParB, we identified variables controlling the translocation velocity, v_{ParB}. In all cases, we find that v_{ParB} is given by the mean rate, k, of disassembly of a ParA filament, so that $v_{\mathrm{ParB}} = ak$, where a is the length of a ParA subunit. In order for a subunit to disassemble from the tip of a ParA filament, the subunit must bind to ParB, its ATP must hydrolyze, and the subunit must fall off. k therefore depends on the distance, ℓ, that the ParB polymer typically penetrates into the ParA bundle and causes ParA-ATP hydrolysis, the rate, k_h, of ParA-ATP hydrolysis, and the rate, k_d, at which a ParA subunit depolymerizes once hydrolyzed.

In turn, the penetration length, ℓ, depends on the shape of the ParB polymer. In our simulations, the freely diffusing ParB polymer adopts an isotropic, globular equilibrium shape. The maximum value, $\ell_{\max}$, of the penetration length, ℓ, is achieved if the ParB polymer is able to maintain this equilibrium shape as it is pulled by ParA. If the disassembly rate, k, is too high, the ParB polymer is pulled along so rapidly that it does not have time to relax to its equilibrium shape. In this case, the ParA bundle pulls the leading region of the ParB polymer faster than the rear of the polymer can respond to the perturbation and the ParB polymer stretches out. Because the part of ParB polymer does not keep pace with the retraction of the depolymerizing ParA bundle, the ParB polymer does penetrate as deeply into the ParA bundle, so $\ell < \ell_{\max}$.

We now estimate the time for the ParB polymer to relax to its equilibrium size. In our simulations, since ParB decorates the center section of the polymer and binds to ParA, the undecorated peripheral segments of the chain are the first ones to stretch out when the ParB polymer is pulled too rapidly (Video S3). The stretching of the peripheral segments is governed by the equation:

$$\langle \dot{z} \rangle = v_{\mathrm{ParB}} - D_s \langle z \rangle / (R_z^0)^2 = v_{\mathrm{ParB}} - \langle z \rangle / \tau_r, \qquad (1)$$

where $\langle z \rangle$ is the ensemble-averaged z-distance between the ends of a peripheral segment pulled by one end in the z-direction, D_s is the diffusion coefficient of the segment, R_z^0 is the z-component of its equilibrium radius of gyration, and the relaxation time, $\tau_r = (R_z^0)^2/D_s$, is the ratio of its internal drag, $k_B T/D_s$, to the effective spring constant, $k_B T/(R_z^0)^2$ (see Text S1). Stretching is appreciable if $\langle z \rangle \gtrsim R_z^0$, so for translocation in steady state ($\langle \dot{z} \rangle = 0$), stretching becomes appreciable for $v_{\mathrm{ParB}} \gtrsim v^* = D_s/R_z^0$, or, equivalently, $akR_z^0/D_s \gtrsim 1$ (inset to Fig. 3a). The shape of the pulled ParB polymer is therefore governed by the product $\tau_a k$, where we have defined

$$\tau_a = aR_z^0/D_s = (a/R_z^0)\tau_r. \qquad (2)$$

The penetration length, ℓ, depends directly on the shape of the ParB polymer. For large $\tau_a k$ the ParB polymer is pulled rapidly and ℓ is small. This is because the ParB polymer is pulled away from the ParA bundle, leading to less overlap of the volume of the ParB polymer with the volume of the ParA bundle. As a result, there is less binding between individual ParB subunits with ParA subunits. As $\tau_a k$ decreases, ℓ increases and saturates at $\ell_{\max}$ for $\tau_a k \lesssim 1$ (inset to Fig. 3b). In the latter regime, the disassembly rate is $k = k_0$, where

$$ak_0 = (1/\ell_{\max} k_h + 1/ak_d)^{-1}. \qquad (3)$$

Thus, the translocation velocity is controlled by the effective relaxation time, τ_a, and the maximum disassembly rate k_0.

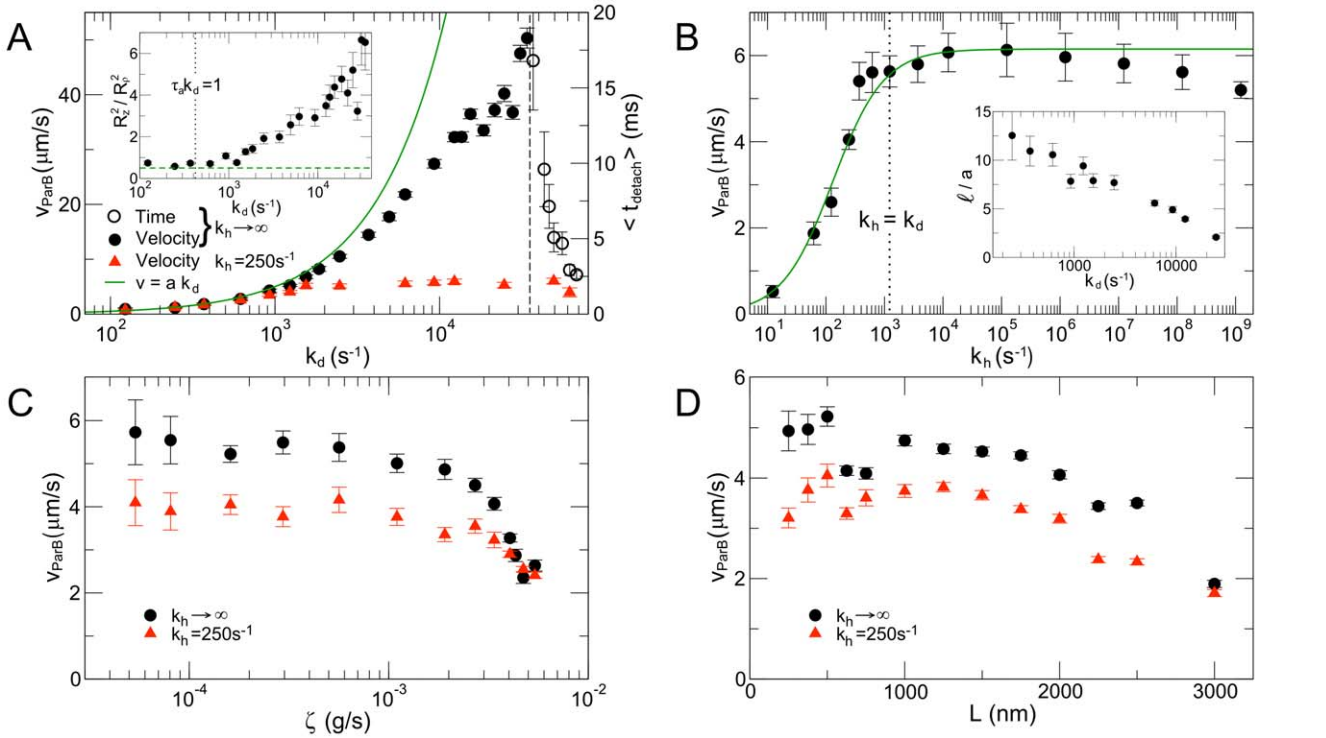

Figure 3. Dependence of translocation velocity on disassembly rate and relaxation time. (A) Translocation velocity, v_{ParB} (solid symbols), increases with depolymerization rate, k_d. At low k_d, v_{ParB} is linear in k_d, scaling as ak_d (green curve), where a is the diameter of a ParA subunit. At large k_d, with an arbitrarily fast hydrolysis rate, k_h, the ParB polymer detaches from the ParA bundle in an observably short time, $\langle t_{\mathrm{detach}} \rangle$ (open symbols). The dashed line separates the regime of translocation from the regime of detachment. For small k_h (red triangles), translocation velocity saturates at intermediate values of k_d and v_{ParB}. *Inset:* Ratio of the z-component of the radius of gyration of the ParB polymer squared to the ρ-component squared (R_z^2/R_ρ^2). At large k_d, the polymer stretches along the axis of motility. The black dotted line marks the k_d at which the depolymerization time, $1/k_d$, exceeds the effective relaxation time, τ_a (Eq. 2), of the ParB polymer. The green dashed line indicates $R_z^2/R_\rho^2 = 1/2$, which is expected for an isotropic polymer coil. (B) v_{ParB} grows with hydrolysis rate for small k_h and saturates at $k_h \approx k_d$ (indicated by dotted line). This behavior can be fit by $1/v_{\mathrm{ParB}} = 1/\ell k_h + 1/ak_d$ (green, see Eq. 3). *Inset:* Variation of the best-fit length scale, ℓ, over ParA subunit diameter, a, with k_d. (C) v_{ParB} is insensitive to the total drag, ζ_{ParB}, on the ParB polymer over several orders of magnitude for both fast k_h (black) and slow k_h (red). For very large ζ_{ParB}, the ParB polymer translocates more slowly. (D) For a fixed quantity of ParB as one component of the polymer, longer polymers move more slowly than shorter polymers for both fast k_h (black circles) and slow k_h (red triangles). Unless noted to be varying, variables have the following values: $k_d = 1230\mathrm{s}^{-1}$, $k_h = \infty$ (black circles) or $k_h = 250\mathrm{s}^{-1}$ (red triangles), $\epsilon = 8k_BT$, $\zeta_{\mathrm{ParB}} = 300\zeta_0 = 1.6{\cdot}10^{-4}\mathrm{g/s}$, $L = 500\mathrm{nm}$, and there are 50 subunits that can bind to ParA in the ParB polymer. In (D), $\zeta_{\mathrm{ParB}} = (5(L/a - 50) + 50)\zeta_0$.
doi:10.1371/journal.pcbi.1002145.g003

Three regimes of translocation velocity

We find that the translocation velocity, v_{ParB}, falls into three regimes, depending on $\tau_a k_0$:

$$v_{\mathrm{ParB}} \begin{cases} \approx ak_0 \text{ for } \tau_a k_0 \lesssim 1 \quad \text{(regime I)} \\ \lesssim ak_0 \text{ for } \tau_a k_0 \gtrsim 1 \quad \text{(regime II)} \\ = 0 \text{ for } \tau_a k_0 \gg 1 \quad \text{(regime III)} \end{cases} \tag{4}$$

For $\tau_a k_0 \lesssim 1$ (regime I), the ParB polymer retains its equilibrium shape as it is pulled across the cell at the velocity $v_{\mathrm{ParB}} = ak_0$. For $\tau_a k_0 \lesssim 1$ (regime II), the ParB polymer stretches as it is pulled and does not penetrate deeply into the ParA bundle. Since fewer ParA subunits bind to ParB, fewer are hydrolyzed and v_{ParB} drops below ak_0. For $\tau_a k_0 \gg 1$ (regime III), the ParB polymer is so elongated that ParB binds to very few ParA subunits and the ParB polymer quickly detaches from the ParA bundle, leading to $v_{\mathrm{ParB}} = 0$.

This physical picture explains the results shown in Fig. 3, where we vary both the disassembly rate, k_0 (Figs. 3a–b) and the effective relaxation time, τ_a (Figs. 3c–d). Specifically, Fig. 3a shows how v_{ParB} depends on the depolymerization rate, k_d. For the black circles in Fig. 3a, the hydrolysis rate, k_h, is effectively infinite so that $k_0 = k_d$ (Eq. 3). In this case, for sufficiently small k_d, the system is in regime I and $v_{\mathrm{ParB}} \approx ak_0 = ak_d$. As k_d increases, $\tau_a k_0 = \tau_a k_d$ also increases; as a result, the ParB polymer stretches (inset to Fig. 3a) and the system crosses into regime II, where v_{ParB} drops below $ak_0 = ak_d$. At very large k_d, the system reaches regime III, and $v_{\mathrm{ParB}} = 0$.

In contrast, if k_h is small (red triangles in Fig. 3a), then k_0 cannot exceed $\ell_{\max} k_h$ as k_d increases (Eq. 3). Therefore, for small k_h, the ParB polymer remains in regime I, $\tau_a k_0 \lesssim 1$, for all k_d, so that $v_{\mathrm{ParB}} \approx ak_0$ and translocation is robust for any k_d. Thus, by decreasing the overall rate of disassembly by lowering k_h, the system can achieve robust translocation, albeit at a cost to velocity.

Fig. 3b shows how v_{ParB} varies as k_h increases. In this case, k_0 saturates to k_d at large k_h (Eq. 3). Since k_d is chosen to be small, we find $\tau_a k_0 \approx 1$ over the entire range of k_h, meaning the system is in regime I and $v_{\mathrm{ParB}} \approx ak_0$.

The different velocity regimes can also be explored by varying τ_a instead of k_0. Fig. 3c shows that v_{ParB} is insensitive to the total drag, $\zeta_{\mathrm{ParB}} = k_BT/D_{\mathrm{ParB}}$, on the polymer when ζ_{ParB} and thus τ_a are small. In this case, $\tau_a k_0$ is small, and the system is in regime I. As ζ_{ParB} increases, $\tau_a k_0$ increases, causing v_{ParB} to drop below ak_0 as the system crosses into regime II.

Fig. 3d shows the effect of the total contour length, L, of the ParB polymer. For small L, $v_{\mathrm{ParB}} \approx ak_0$ is constant since the system is in regime I. As L increases, τ_a increases, a9nd when $\tau_a k_0 \gtrsim 1$, v_{ParB} crosses into regime II and v_{ParB} drops below ak_0.

Dependence of the translocation velocity on binding energy, binding sites, applied load, and other physical variables

Fig. 4 shows that v_{ParB} has a threshold dependence on the ParB–ParA binding energy, ϵ. As shown in Figs. 2c, 4, ParB rapidly detaches from the ParA bundle if ϵ is too small. However, as long as ϵ is sufficiently large, the ParB polymer remains attached to the bundle throughout the simulation and translocates with a velocity that is insensitive to ϵ and is set by $\tau_a k_0$ (Eq. 4). We observe similar behavior as the number of binding sites on the ParB polymer is varied. If there are too few binding sites, the ParB polymer quickly detaches from ParA. Above a threshold value, however, v_{ParB} does not sensitively depend on the length of the binding strip (Fig. S1). The translocation velocity is also insensitive to the filament density within the ParA bundle, the arrangement of filaments in the bundle, and stiffness of the ParB polymer (Figs. S2, S3, S4). Finally, we have also verified that our main results hold when the form of the ParB–ParA binding potential is altered to allow binding by multiple points on ParB and/or ParA subunits.

Detachment force for the ParB polymer

We next investigate the extent to which motility is robust to an external force on the ParB polymer that opposes translocation. The external force, $f_{\mathrm{ext}}/2$, opposes translocation by pulling on each end of the ParB polymer. In our simulations, we find that v_{ParB} is unperturbed for $f_{\mathrm{ext}} \lesssim f^* \approx 10\mathrm{pN}$ (Fig. S5). For $f_{\mathrm{ext}} > f^*$, however, the ParB polymer rapidly detaches from the ParA bundle and translocation stalls.

In order to understand this behavior, we analytically estimate the "detachment force," f^*, required to pull the ParB polymer off of the ParA bundle in a time, τ^*, that is approximately equal to the time required for the ParB polymer to translocate across the cell (see Text S1 for details).

In our simulations, we model the ParB-*parS-ori* complex as a polymer chain comprised of N monomeric subunits. Each subunit in the central strip of the ParB polymer binds with a binding energy, ϵ, to a subunit in the ParA bundle. Thus, the total strength

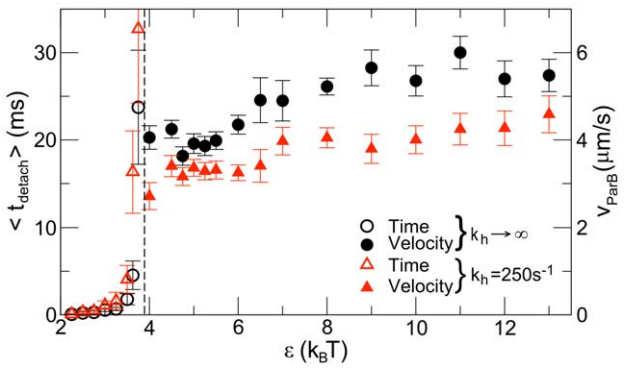

Figure 4. Dependence of translocation velocity on ParB–ParA binding energy. ParB detaches in an observably short time, $\langle t_{\mathrm{detach}} \rangle$, when the binding energy, ϵ, is too small (open symbols). When ϵ is large enough, v_{ParB} (solid symbols) is non-zero, and is insensitive to ϵ over the observed range for both fast (black) and slow (red) k_h. The dashed line separates regimes of detachment and translocation.
doi:10.1371/journal.pcbi.1002145.g004

of the attraction between the ParB polymer and the ParA bundle is approximately proportional to $n\epsilon$, where n is the number of ParB subunits actually bound to ParA. Since ParB subunits lie in approximately a Gaussian distribution about the center of mass of the ParB polymer [34], $n = n(z_{\mathrm{cm}})$, depends on the location, z_{cm}, of the center of mass of the ParB polymer.

Now consider the effect of a force $-f\hat{z}$ on the ParB polymer that opposes translocation in the $\hat{z}$ direction. At the simplest level, based on the above analysis, the ParB polymer may be replaced by a point particle at the center of mass of the ParB polymer, z_{cm}, in an effective potential given by

$$U(z_{\mathrm{cm}}) = -\epsilon n(z_{\mathrm{cm}}) + f z_{\mathrm{cm}}. \quad (5)$$

The first term is due to ParB binding to ParA and the second term is the work done by the external pulling force, f. As f increases, the minimum of U shifts to lower values of z_{cm} and the number of bound ParB sites decreases, eventually leading to unbinding of the ParB polymer from the ParA bundle.

The mean time for the particle to escape from the potential well (to detach from the ParA bundle) is well approximated by the Kramers escape time, τ_{K} for this potential [35,36]:

$$\tau_{\mathrm{K}} = \frac{2\pi k_B T}{D} |U''(z_{\min}) U''(z_{\max})|^{-1/2} e^{(U(z_{\max}) - U(z_{\min}))/k_B T}. \quad (6)$$

Given these expressions, we calculate the detachment force f^* to be the force f for which the escape time, τ_K, is equal to τ^*, the time required for the ParB polymer to translocate across the cell.

In simulations with our standard model, the central binding strip has $R = 16\mathrm{nm}$ and $D = 0.054\ \mu\mathrm{m}^2/\mathrm{s}$. There are $N = 50$ ParB subunits that bind to ParA with energy, $\epsilon = 8k_B T$, so the maximum total binding energy is $N\epsilon = 400k_B T$. The ParB polymer translocates at $v_{\mathrm{ParB}} = 5\mu\mathrm{m/s}$, so that the time to translocate $1\mu\mathrm{m}$ is $\tau^* = 200\mathrm{ms}$. With these parameters, we estimate that the detachment force is $f^* \approx 40\mathrm{pN}$. An estimate for the detachment force under more realistic conditions (*in vivo*) is given in the Discussion section.

This order of magnitude estimate agrees with our simulations at high depolymerization rates, k_d (Fig. 3a), large drag coefficients, ζ_{ParB} (Fig. 3c), and large external pulling forces, f_{ext} (Fig. S5). In the first case, the mean time to first detachment is shorter than the translocation time for $k_d \gtrsim 3.4 \cdot 10^5 \mathrm{s}^{-1}$; this suggests that the force, f, required for rapid detachment is $f^* \approx \zeta_{\mathrm{ParB}} v_{\mathrm{ParB}} \approx 10\mathrm{pN}$. Similarly, we find that the ParB polymer fails to translocate for $\zeta_{\mathrm{ParB}} \gtrsim 5.4 \cdot 10^{-3} \mathrm{g/s}$, giving a detachment force of $f^* \approx 15\mathrm{pN}$. In addition, we have conducted simulations in which we apply an external force, $f_{\mathrm{ext}}/2$, to each of the ends of the polymer. For these simulations, we find robust translocation up to a detachment force of $f^* \approx 10\mathrm{pN}$.

The ParB polymer translocates even when the ParA bundle is not anchored

So far, we have assumed that the ParA bundle is anchored to the pole. Recent reports suggest that in *C. crescentus*, ParA is localized to the swarmer pole by TipN [10,12], but it is unclear if TipN actually anchors ParA. We therefore examined whether ParB translocation could occur if the ParA bundle is localized but not anchored.

Fig. 5 shows that the ParB polymer translocates even when the ParA bundle is unanchored. We understand this through Newton's third law, which dictates that the force, F_{BA}, that pulls ParB to ParA is equal in magnitude but opposite in direction to the force

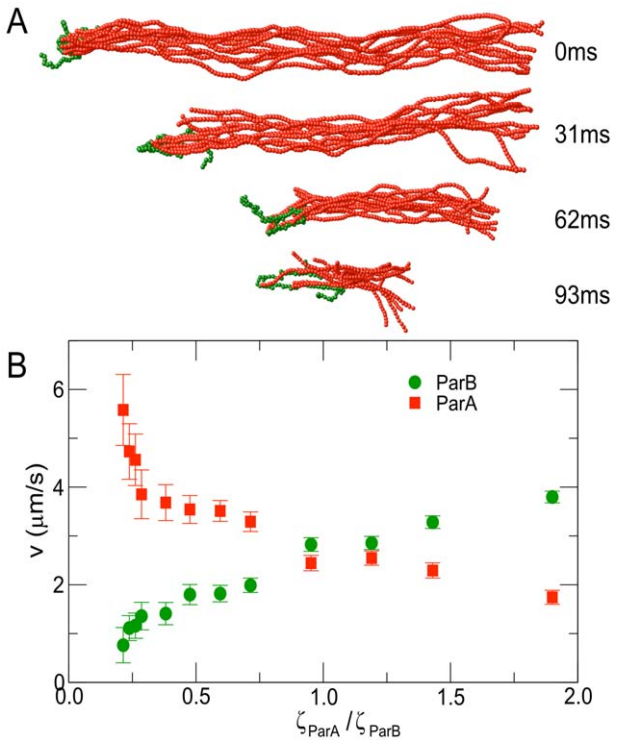

Figure 5. The ParB polymer translocates even when the ParA bundle is unanchored. (A) Snapshots of a simulation in which the ParA bundle is not anchored at its right end (swarmer pole). The ParA bundle (red) is pulled towards mid-cell as the ParB (green) moves towards the swarmer pole. (B) Dependence of speeds of ParA (red) and ParB (green) on the ratio of drags, $\zeta_{ParA}/\zeta_{ParB}$. In these simulations, $\zeta_{ParB}=1.1\cdot10^{-3}$g/s and $L=1000$nm.
doi:10.1371/journal.pcbi.1002145.g005

on ParA. Thus ParB is pulled towards the swarmer pole while ParA is simultaneously pulled away from it:

$$F_{BA}=\zeta_{ParB}v_{ParB}=-\zeta_{ParA}v_{ParA}, \quad (7)$$

where ζ_{ParB} and ζ_{ParA} are the drag coefficients of the ParB polymer and ParA filament bundle, respectively.

In the case of a long, unanchored ParA bundle, $\zeta_{ParA}\gg\zeta_{ParB}$ and the ParB polymer translocates across the cell while the ParA bundle remains relatively stationary (Fig. 5b). However, if the ParA bundle is sufficiently small (*e.g.*, when the ParB has nearly reached the swarmer pole), $\zeta_{ParA}/\zeta_{ParB}$ is small, so the large ParB polymer remains relatively stationary while pulling the smaller, disassembling ParA bundle towards mid-cell (Fig. 5b).

Discussion

Based on recent experimental observations [7–12,15], we have tested several simulation models (Fig. 2) and discovered a robust mechanism for chromosome segregation in *C. crescentus* via the ParABS system.

Self-diffusiophoresis can explain ParA pulling

Our simulations point to a specific physical mechanism underlying translocation in the ParABS system. We find that disassembly of ParA generates a steady-state ParA filament concentration gradient that remains fixed in the center-of-mass frame of the translocating ParB polymer (Fig. 1c). In other words, disassembly of ParA allows the ParA filament concentration gradient to translocate with the particle across the cell so that at all times the ParB polymer is moving up the concentration gradient of ParA to satisfy its attraction to ParA. Our simulations do not include fluid flow, but it is known that external concentration gradients can also drive motion of a particle in a fluid environment; the latter phenomenon is known as "diffusiophoresis." If the particle (in this case, the ParB-*parS*-*ori* complex) is attracted to the solute (the ParA filament bundle), it will translocate up the concentration gradient towards high solute concentrations [37]. In "self-diffusiophoresis," the particle itself (the ParB-*parS*-*ori* complex) generates and sustains the solute concentration gradient [38,39] via disassembly of ParA. We emphasize that ParB-induced depolymerization (particle-induced destruction of solute) is central to this process. Without depolymerization, the ParA bundle would remain intact and the concentration of ParA filaments would not change with time. As a result, the ParA concentration profile would not be able to move with the particle and translocation would not occur.

This intrinsically many-body mechanism is distinct from biased diffusion. In contrast to biased diffusion mechanisms which apply to a coupler that attaches a load to a single filament or fiber [20–22,26], self-diffusiophoretic translocation can occur even if the ParB polymer does not diffuse, as long as the ParB-ParA interaction range is finite. In self-diffusiophoresis, "diffusio" refers not to diffusion of a coupler, but to the key role of the solute gradient, just as the prefix in "electrophoresis" refers to an electric potential gradient [37]. The self-diffusiophoretic mechanism also differs from ones involving motion of a coupler [3,20–27]; in our case, the load is not attached to a coupler that cannot detach from the depolymerizing filaments. Instead, the load is attached directly to the depolymerizing filaments via many non-permanent bonds.

It has been suggested that polymerization-driven motility, as in the case of F-actin in the lamellipodium of eukaryotic cells, also constitutes an example of self-diffusiophoretic motility [40,41]. In that case, the object to be moved (*e.g.*, the cell membrane) is repelled by the structure (the branched actin network) that it builds in order to move. In depolymerization-driven translocation, on the other hand, the object to be moved (the ParB-DNA complex) is attracted to the structure (ParA) that it destroys in order to move.

The self-diffusiophoretic mechanism suggests modes of failure for translocation. For example, overexpression of ParA leads to segregation defects, and it has been suggested that these defects arise due to the increase in the quantity of delocalized ParA [12,15]. This effect may be analogous to what we observe in our simulations with severing (Video S2), where instead of binding to the ParA bundle, ParB can bind to severed ParA filaments. This disrupts the steady-state generation of a translating ParA concentration gradient so that it does not support steady-state ParB polymer translocation. Similarly, when ParA is overexpressed, extra ParA monomers or protofilaments may diminish or erase the ParA concentration gradient created by depolymerization. Alternatively, the extra ParA could saturate ParB, preventing translation of the ParA gradient.

Translocation is most robust for side-binding of ParB to ParA with disassembly only from the tip

We observe robust translocation over a wide range of physical parameters only if ParB binds to the sides of ParA filaments, triggering disassembly only from the tips of filaments (Fig. 1b–c). If ParB binds only to the tips of filaments, translocation is far less robust for two reasons. First, there are many fewer ParA subunits to which ParB can bind so the overall attraction between ParB and ParA is weaker. Second, the ParB polymer is localized near the tip

of the bundle, at the very edge of the concentration gradient of ParA that drives translocation. In contrast, in the side-binding model, the ParB polymer penetrates further into the bundle so that it is localized near the steepest, central section of the concentration gradient (Fig. S6). Thus, in the tip-binding-only model, the ParB polymer is much more likely to detach from the ParA bundle due to thermal noise (Fig. 2a). This failure mode can only be averted by greatly increasing the binding energy or the number of filaments, and thus tips, in the ParA bundle.

We also find that ParA disassembly via severing does not provide robust translocation (Fig. 2b) because severed protofilaments can bind to ParB, reducing the attraction between the ParB polymer and the main ParA bundle, leading to detachment.

We therefore predict that ParB binds to the sides of ParA filaments and ParA filaments disassemble primarily from the tip. This prediction can be tested with *in vitro* experiments.

Comparisons with experiments on Par-mediated chromosome pulling

Our model is sufficiently versatile to account for a range of experimental observations. For example, by varying the initial density and cross-linking of the ParA filament bundle in our simulations, we find cases in which some ParA filaments remain partially assembled even though the ParB polymer has translocated across the cell (Fig. S7). This is in agreement with the observations of Ptacin *et al.* [10], who found that in some cases, a fiber of ParA extended across the predivisional cell after *ori* had translocated.

We find that the robustness of translocation is primarily controlled by the quantity $\tau_a k_0$, the product of an effective relaxation time (Eq. 2) and the maximum rate of disassembly of ParA (Eq. 3). The underlying details of the ParB polymer are only important insofar as they affect quantitative results such as the precise value of the relaxation time; they do not affect the qualitative physical principles described above.

Specifically, if $\tau_a k_0$ is too high, the ParB polymer stretches out and can detach from the ParA bundle. This finding suggests a possible role for chromosome organizing factors such as the SMC protein [14,42]. In order to translocate reliably and efficiently, the chromosome of four million base pairs [14,16] must be organized such that it does not overload the pulling mechanism. We propose that one important physical function of chromosomal organization and condensation is to minimize the effective relaxation time, τ_a, so that the chromosome can keep up with the retracting ParA bundle, to ensure robust translocation.

In addition, we find that the velocity is simply the product of the ParA subunit length and the maximum disassembly rate, k_0, provided disassembly is slow enough to guarantee that $\tau_a k_0 \lesssim 1$ (Eq. 4). From the observed *ori* translocation velocity, $v = 0.3\ \mu\mathrm{m/min}$ [9,11,16,17], we estimate the *in vivo* ParA disassembly rate to be $k \approx 0.9\mathrm{s}^{-1}$, which is slower than the measured disassembly rate of dynamically unstable ParM filaments [43], but comparable to the disassembly rate of actin filaments [44].

The translocation velocity in our simulations is considerably higher, typically several $\mu\mathrm{m/s}$, because we used high disassembly rates. Translocation is robust in our simulations at these high values of k_0 because the effective relaxation time, τ_a, of our ParB polymer is fairly short. In the real system, where the effective relaxation time of the chromosome is likely to be considerably longer, it could be a biological necessity that both ParA disassembly and *ori* translocation proceed at slower than the simulated rates.

Likewise, in our simulations the ParB polymer detaches when it is pulled with a force f^* of order tens of pN, but this detachment force is likely to be much higher in the real system. The most important difference between our simulations and the actual bacterium lies in the number of ParB binding sites N. To estimate the detachment force, f^*, under realistic conditions, we first estimate N, the maximum possible binding energy $N\epsilon$, the extent of the chromosome R, and the diffusion coefficient of the chromosome D. We first estimate $N \approx 1000$ by assuming that ParB decorates the approximately 10 kilobase segment of the chromosome that was found to be the site of force exertion during translocation in [9]. For $\epsilon \approx 10 k_B T$ we therefore obtain a maximum binding energy of $N\epsilon \approx 10^4 k_B T$. For ideal polymer chains [34], $R_z \propto \sqrt{N}$ and $D \propto 1/N$. Thus, we estimate $R_z \approx 100\mathrm{nm}$ and $D \approx 10^{-3}\ \mu\mathrm{m}^2/\mathrm{s}$. This crude estimate of R actually agrees well with experimental snapshots of *C. crescentus* during chromosome segregation [10,11]. The estimate of D falls within the range $10^{-1}\ \mu\mathrm{m}^2/\mathrm{s} < D < 10^{-5}\ \mu\mathrm{m}^2/\mathrm{s}$, which is measured in *E. coli* for DNA segments of varying sizes [45,46]. We note that f^* is insensitive to D, and varies by less than $1\mathrm{pN}$ over that range.

According to experiments [9,11,16,17], the ParB-*parS-ori* complex translocates across the cell in about 10 minutes. Using Eq. 6, we find that the detachment force is $f^* \approx 200\mathrm{pN}$. This value is of the same order of magnitude as the $700\mathrm{pN}$ stall force for chromosome segregation along kinetochore fibers in eukaryotes [47,48]. Thus, this estimate suggests that the mechanism we have proposed is both physically reasonable and biologically relevant.

Implications for other phenomena

Insights from our results may extend to plasmid segregation by ParAB. In *Escherichia coli*, the ParA concentration profile is known to oscillate as plasmid pB171 is partitioned [6,19,49]. This dynamic behavior appears to be required for proper plasmid partitioning [7,19]. We suggest that ParB creates a moving ParA filament concentration gradient that pulls the plasmid along as ParA disassembles.

In addition, our findings suggest an alternative explanation for observations that the distance that plasmid pB171 translocates in a given time interval increases approximately linearly with the initial ParA filament length [7]. Ringgaard *et al.* [7] suggest that this effect arises from a ParA filament-length-dependent plasmid detachment rate. However, we have shown that the relative velocities of the ParB polymer and the ParA bundle depend on the ratio of the viscous drags on ParA and ParB, $\zeta_{\mathrm{ParA}}/\zeta_{\mathrm{ParB}}$ (Fig. 5). Thus, the observed dependence of plasmid translocation distances and velocities on ParA filament length may simply be a result of Newton's third law, due to the variation of $\zeta_{\mathrm{ParA}}/\zeta_{\mathrm{ParB}}$ with ParA filament length.

Our simulations with unanchored ParA filaments suggest a new possibility for the mechanism of terminus segregation in *C. crescentus*. As translocation begins, the ParA filaments are long, so $\zeta_{\mathrm{ParA}} > \zeta_{\mathrm{ParB}}$ and the ParB polymer is pulled rapidly towards the swarmer pole. However, as the ParB polymer nears the swarmer pole the ParA filaments are much shorter and $\zeta_{\mathrm{ParA}} < \zeta_{\mathrm{ParB}}$ may be satisfied, so that the ParA bundle is pulled toward mid-cell. Experiments have indicated that ParA binds non-specifically to DNA [7,10,18]. Thus, we propose that DNA near the terminus is non-specifically bound to ParA and translocates away from the swarmer pole as ParA filaments are pulled toward mid-cell by the ParB-*parS-ori* complex. In contrast to previously suggested passive mechanisms [16,30,33], this is an active process, directly linked to *ori* translocation.

Our results provide a new paradigm for understanding depolymerization-driven translocation in prokaryotic DNA segregation systems. Since self-assembly and disassembly are ubiquitous in cellular systems, the creation of concentration gradients by these processes provides a general and robust mechanism for translocation.

Methods

At the start of each simulation, ParA monomeric subunits form a cross-linked bundle of filaments. The ParB-decorated chromosome is represented by a semi-flexible chain of monomeric subunits, typically of length 100 subunits, divided into three sections. The center section, typically of length 50 subunits, represents the part of the chromosome bound to ParB; these subunits can bind specifically to ParA subunits. The two end sections of the ParB polymer flanking the ParB section do not bind to ParA.

Biochemistry

The process of ParA disassembly begins when a ParB subunit binds to a ParA-ATP subunit. If the interaction energy, U_{AB}, exceeds a certain threshold, 0.75ϵ, the ParA-ATP hydrolyzes at rate k_h. Once the ParA subunit hydrolyzes, it may detach from the ParA filament by depolymerization at rate k_d (after which it continues to interact with other subunits by the interaction U_R). In our standard model, ParB binds to the sides of ParA filaments, and a hydrolyzed ParA subunit can only depolymerize if it is located at the tip of a ParA filament.

Units

Simulation units are converted into physical units by taking the subunit length to be $a = 5\text{nm}$. The typical subunit diffusion coefficient is taken to be $D = 7.7\ \mu\text{m}^2/\text{s}$, as measured in [50], and the diffusion coefficient for a particular subunit is $D_i = D/\zeta_i$ (typically $\zeta_i = 1$ or 5, see below), giving a cell viscosity $\eta = 11.4\text{cP}$ and a characteristic time scale $\tau = a^2/D = 3.3\ \mu\text{s}$. Typical runs are approximately 100ms and simulation steps are 0.81ns.

Interactions

Several interactions are included in the model; their specific forms are given below. All subunits are spheres with diameter a that repel each other if they overlap:

$$U_R(r_{ij}) = \begin{cases} \frac{1}{2}K_R(r_{ij}-a)^2, & \text{for } r_{ij} < a \\ 0 & \text{for } r_{ij} \geq a, \end{cases} \quad (8)$$

where r_{ij} is the center-to-center distance between subunits i and j and $K_R = 100k_BT/a^2$. Within a ParA or ParB polymer chain, neighboring subunits are held together through an attractive harmonic potential:

$$U_B(r_{ij}) = \frac{1}{2}K_B(r_{ij}-a)^2, \text{ for } r_{ij} > a, \quad (9)$$

with $K_B = 100k_BT/a^2$. In order to hold the ParA bundle together, we typically take 40% of ParA subunits to be cross-linked to a subunit in a nearby filament through an attractive potential:

$$U_C(r_{ij}) = \frac{1}{2}K_C(r_{ij}-b)^2, \text{ for } r_{ij} > b, \quad (10)$$

where $b = 5a$ is the initial spacing of filaments in the ParA bundle and $K_C = K_B/2$. ParA filaments are stiffened by a bending potential [51]:

$$U_S(\theta_i) = \frac{1}{2}K_S(\cos\theta_i - \cos\theta_0)^2, \quad (11)$$

where θ_i is the angle between the bond vector, $\vec{b}_{i-1,i}$, between ParA subunits $i-1$ and i, and the bond vector, $\vec{b}_{i,i+1}$, between subunits i and $i+1$. Thus, $\cos\theta_i = \hat{b}_{i-1,i}\cdot\hat{b}_{i,i+1}$, where $\hat{b} = \vec{b}/|\vec{b}|$. We take $K_S = 500k_BT$ and $\theta_0 = 0$. Similarly, the stiffness of the ParB polymer can be controlled by an interaction potential of form of Eq. 11 (however, in our standard model, $K_S = 0k_BT$ in the ParB polymer).

In addition, we introduce interactions so that binding between ParA and ParB occurs in specific spatial locations on the spheres representing the subunits. Each subunit i has a unit polarization vector, $\hat{p}_i$, that determines the location of the binding site for the ParB–ParA interaction, and the following interaction potential aligns it to be at an angle θ_p to the bond vectors $\vec{b}$ connecting adjacent subunits:

$$U_P(\theta_i) = \frac{1}{2}K_P(\hat{p}_i\cdot\hat{b}_{i,i+1} - \cos\theta_p)^2 + \frac{1}{2}K_P(\hat{p}_i\cdot\hat{b}_{i-1,i} - \cos\theta_p)^2. \quad (12)$$

We choose $\theta_p = \pi/2$ so that $\hat{p}_i$ tends to be perpendicular to the bond vectors, and fix $K_P = 100k_BT$ for ParA filaments and $K_P = 25k_BT$ in the ParB polymer, which is relatively more flexible. Binding sites are arranged helically on the ParA filaments and the ParB polymer due to two additional interaction potentials. The first constrains polarization vectors on nearest-neighbor subunits on a given chain:

$$U_{H1}(\psi_{i,1}) = \frac{1}{2}K_{H1}(\cos\psi_{i,1} - \cos\psi_{01})^2, \quad (13)$$

where $\cos\psi_{i,1} \equiv \hat{p}_i\cdot\hat{p}_{i+1}$ and $\psi_{01} = \pi/18$ sets the pitch of the helix. Here, $K_{H1} = 200k_BT$ for ParA and $K_{H1} = 50k_BT$ for ParB. The second potential has the same form,

$$U_{H2}(\psi_{i,2}) = \frac{1}{2}K_{H2}(\cos\psi_{i,2} - \cos\psi_{02})^2, \quad (14)$$

but constrains polarization vectors on the next-nearest-neighbor subunits with $\cos\psi_{i,2} \equiv \hat{p}_i\cdot\hat{p}_{i+2}$ and $\psi_{02} = \pi/9$. Here, $K_{H2} = 100k_BT$ in ParA and $K_{H2} = 25k_BT$ for ParB. Note that in addition to regulating the locations of the binding sites, Eqs. 13 and 14 implicitly regulate torsion within the ParB polymer.

Finally, ParB binds to ParA with a site-specific, short-ranged interaction potential:

$$U_{AB}(r_{AB},\phi_1,\phi_2,\phi_3) = \begin{cases} \frac{\epsilon}{C}[\frac{\sigma^{14}}{r_{AB}^{14}} - \frac{\sigma^{12}}{r_{AB}^{12}}](\cos\phi_1\cos\phi_2\cos\phi_3)^2 \\ \quad \text{for } \cos\phi_1 > 0,\ \cos\phi_2, \cos\phi_3 < 0 \\ 0 \quad \text{otherwise.} \end{cases} \quad (15)$$

where $\vec{r}_{AB} = \vec{r}_B - \vec{r}_A$ is the vector distance between the ParA and ParB subunits and ϵ is the binding energy. In our standard model, $\epsilon = 8k_BT$. The normalization factor $C = (\sigma/a)^{12} - (\sigma/a)^{14}$ ensures that ϵ is the relevant energy scale for binding. The distance $\sigma = a\sqrt{6/7}$ sets $r_{AB} = a$ as the minimum of the binding potential. Binding site specificity is implemented through regulation of the

angles between the polarization vectors on the ParA and ParB subunits as well as $\hat{r}_{AB}=\vec{r}_{AB}/r_{AB}$. In Eq. 15, $\cos\phi_1=\hat{p}_A\cdot\hat{r}_{AB}$, $\cos\phi_2=\hat{p}_B\cdot\hat{r}_{AB}$, and $\cos\phi_3=\hat{p}_A\cdot\hat{p}_B$. Binding is strongest when the two polarization vectors point towards each other and along $\vec{r}_{AB}$.

We have also studied several variations of these models. For example, in a separate set of simulations, we set $K_{H1}=0$ and $K_{H2}=0$ for both ParA and ParB, so that the binding sites were not arranged helically on the ParA filaments and ParB polymer. The orientation of the polarization vectors was set by U_P, where $\theta_p=0$ for tip binding and $\theta_p=\pi/2$ for side-on binding. We also studied cases in which monomeric ParB subunits did not possess specific orientations (polarization vectors). In these cases, ParA polarization vectors were set by U_P, where $\theta_p=0$ for both tip-binding and side-binding. Binding only weakly depended on the orientation of the ParA-ParB bond through a modified version of U_{AB}, which we denote U^*_{AB} and U^{**}_{AB} for tip-binding and side-binding, respectively. For tip-binding without ParB polarization vectors:

$$U^*_{AB}(r_{AB},\phi_1)=\begin{cases}\frac{\epsilon}{C}[\frac{\sigma^{14}}{r^{14}_{AB}}-\frac{\sigma^{12}}{r^{12}_{AB}}]\cos^6\phi_1 \\ \quad \text{for } \cos\phi_1>0 \\ 0 \quad \text{otherwise}\end{cases} \tag{16}$$

For side-binding without ParB polarization vectors::

$$U^{**}_{AB}(r_{AB},\phi_1)=\frac{\epsilon}{C}[\frac{\sigma^{14}}{r^{14}_{AB}}-\frac{\sigma^{12}}{r^{12}_{AB}}]\sin^{10}\phi_1 \tag{17}$$

where r_{AB}, ϕ_1, σ, and C are as defined above.

Equations of motion

All subunits in the system translate and rotate according to Brownian dynamics [52]. Thus, we solve a system of coupled Langevin equation where the velocity of each subunit is governed by the forces exerted by other subunits in the system as well as thermal forces, $\vec{F}$ from the surrounding liquid medium:

$$\zeta\dot{\vec{r}}=-\vec{\nabla}_r(U_R+U_B+U_C+U_S+U_P+U_{AB})+\vec{F}(t) \tag{18}$$

$$\langle\vec{F}(t)\rangle=0,\ \langle\vec{F}(t)\cdot\vec{F}(t')\rangle=6k_BT\zeta\delta(t-t') \tag{19}$$

and

$$\zeta_p\dot{\hat{\boldsymbol{p}}}=-\vec{\nabla}_p(U_P+U_{H1}+U_{H2}+U_{AB})+\vec{G}(t) \tag{20}$$

$$\langle\vec{G}(t)\rangle=0,\ \langle\vec{G}(t)\cdot\vec{G}(t')\rangle=\frac{a^2}{3}\langle\vec{F}(t)\cdot\vec{F}(t')\rangle=6k_BT\zeta_p\delta(t-t') \tag{21}$$

The subunit friction constant is $\zeta=3\pi\eta a\zeta_i$, where η is the viscosity, and ζ_i is a constant that determines the relative magnitude of the drag on subunit i. Typically, $\zeta_i=1$ for ParA and normal ParB subunits, and $\zeta_i=5$ for ParB subunits that cannot bind to ParA. $\zeta_p=\pi\eta a^3\zeta_i$ is the rotational friction coefficient.

Supporting Information

Figure S1 Behavior of the ParB polymer as a function of the length of the central ParB strip that binds to ParA. If too few of the ParB can bind to ParA, the ParB polymer detaches in an observably finite average time, $\langle t_{\text{detach}}\rangle$ (open symbols). When the percentage of binding sites is above threshold, the translocation velocity, v_{ParB}, is non-zero. If there are enough binding sites to cause disassembly at all of the ParA filament tips simultaneously, v_{ParB} is insensitive to the number of ParB that can bind ParA. The dashed line separates the regimes of detachment and translocation.
(PDF)

Figure S2 Dependence of translocation velocity, v_{ParB}, on the density of ParA filaments within the ParA bundle. For ParA bundles of equal diameter, $d\approx 6a$, but different numbers of ParA filaments, the translocation velocities are approximately equal. Thus, v_{ParB} is insensitive to the density of filaments in the ParA bundle.
(PDF)

Figure S3 Snapshots of a simulation with a ''ParA tube''. The ParA filaments in the ParA bundle are arranged cylindrically. The snapshots are slightly rotated into the page and the thin black circle indicates the base of the cylinder. Translocation of the ParB polymer is insensitive to whether the ParA filaments are arranged as a tube or as a bundle. Depolymerized ParA monomers are not shown.
(PDF)

Figure S4 Dependence of translocation velocity, v_{ParB}, on the stiffness of the ParB polymer. In our standard model, the ParB polymer is flexible, and the bending stiffness is $K_S=0k_BT$. In order to simulate a stiff ParB polymer, we apply the bending potential in Eq. 11 to the ParB polymer. v_{ParB} is insensitive to the bending stiffness over the observed range of K_S.
(PDF)

Figure S5 Force-velocity relation for ParB polymer translocation in our simulations. In these simulations, an external force, $f_{\text{ext}}/2$, pulls on each of the two ends of the ParB polymer, thus opposing depolymerization-driven translocation. Translocation of the ParB polymer is unperturbed when subjected to external pulling forces up to $f_{\text{ext}}\approx 7\text{pN}$.
(PDF)

Figure S6 Steady-state ParA concentration profiles for tip-binding-only and side-binding models. Steady-state ParA concentration is plotted versus position relative to the center of mass of the ParB polymer, which is located at $z=0\text{nm}$ and indicated by the dotted green line. When ParB binds only to the tips of ParA filaments, the center of mass of the ParB polymer (dotted green line) localizes near the edge of the ParA filament concentration gradient (dashed black curve). This enables the ParB polymer to easily escape the ParA concentration gradient and detach from the ParA bundle due to thermal noise. However, when ParB can bind to the sides of ParA filaments, the ParB polymer penetrates further into the ParA bundle, and thus the center of mass (green) of the ParB polymer is localizes near the center of the ParA concentration gradient (dashed red curve). Thus, the ParB polymer is not susceptible to falling out of the ParA gradient and detaching from the ParA bundle due to thermal noise.
(PDF)

Figure S7 Snapshots of a simulation in which several ParA filaments remain after the ParB polymer has translocated. If the initial spacing, b, of the ParA filaments in the bundle is large, the ParB polymer may translocate by disassembling some, but not all, of the ParA filaments. In the

snapshots shown, the initial ParA filament spacing is $b = 20a$, four times greater than the initial spacing, used in our standard simulations. This simulation demonstrates the versatility of our model by replicating one of the observations of Ptacin *et al.* (2010) [10]. This result can also be obtained with closely packed (*e.g.*, $b = 5a$) ParA filaments if the filament bundle contains a large number of filaments.
(PDF)

Text S1 Polymer relaxation time and estimated detachment force for the ParB polymer. This text explains how to calculate the characteristic polymer relaxation time, τ_r, and the peripheral segment diffusion coefficient, D_s. In addition, we provide details for the estimation of the detachment force, f^*.
(PDF)

Video S1 A movie of translocation of the ParB polymer in our standard simulation conditions. The ParB polymer remains localized near the tip of the ParA bundle and translocates as the ParA bundle disassembles. Depolymerized ParA monomers are not shown.
(MOV)

Video S2 A movie of a simulation run for the model in which ParB binds to the sides of ParA filaments and severs them. The ParB polymer translocates briefly until severed ParA protofilaments bind to the ParB polymer and disrupt its binding to the main ParA filament bundle.
(MOV)

Video S3 Stretching of the ParB polymer. When the maximum ParA disassembly rate, k_0, is sufficiently large, the ParB polymer does not have time to relax to its equilibrium shape as it is pulled, and therefore stretches out. The ParB polymer consists of three segments; the two peripheral segments (light green), which cannot bind to ParA, and the central segment (dark green), which can bind to ParA. Note that the peripheral segments of the ParB polymer stretch, while the central segment of the ParB polymer is initially bound to the ParA filament bundle. When the peripheral segments stretch too far, they start to stretch the central segment, thus decreasing the length, ℓ, that the ParB polymer penetrates into the ParA bundle. This can lead to detachment for sufficiently high k_0. In this movie, $k_0 = k_d = 6170\mathrm{s}^{-1}$, five times greater than the ParA disassembly rate, k_0, in our standard simulations (see Fig. 3 caption).
(MOV)

Acknowledgments

We thank Rob Phillips for helpful discussions.

Author Contributions

Conceived and designed the experiments: EJB ZG NSW AJL. Performed the experiments: EJB MAG. Analyzed the data: EJB. Wrote the paper: EJB NSW AJL.

References

1. Mitchison T, Kirschner M (1984) Dynamic instability of microtubule growth. Nature 312: 237–242.
2. Walczak CE, Cai S, Khodjakov A (2010) Mechanisms of chromosome behaviour during mitosis. Nat Rev Mol Cell Biol 11: 91–102.
3. McIntosh JR, Volkov V, Ataullakhanov FI, Grishchuk EL (2010) Tubulin depolymerization may be an ancient biological motor. J Cell Sci 123: 3425–3434.
4. Gerdes K, Howard M, Szardenings F (2010) Pushing and pulling in prokaryotic DNA segregation. Cell 141: 927–942.
5. Kirkpatrick CL, Viollier PH (2010) A polarity factor takes the lead in chromosome segregation. EMBO J 29: 3035–3036.
6. Ebersbach G, Gerdes K (2001) he double *par* locus of virulence factor pB171: DNA segregation is correlated with oscillation of ParA. Proc Natl Acad Sci USA 98: 15078–15083.
7. Ringgaard S, van Zon J, Howard M, Gerdes K (2009) Movement and equipositioning of plasmids by ParA filament disassembly. Proc Natl Acad Sci USA 106: 19369–19374.
8. Fogel MA, Waldor MK (2006) A dynamic, mitotic-like mechanism for bacterial chromosome segregation. Genes Dev 20: 3269–3282.
9. Toro E, Hong SH, McAdams HH, Shapiro L (2008) *Caulobacter* requires a dedicated mechanism to initiate chromosome segregation. Proc Natl Acad Sci USA 105: 15435–15440.
10. Ptacin JL, Lee SF, Garner EC, Toro E, Eckart M, et al. (2010) A spindle-like apparatus guides bacterial chromosome segregation. Nat Cell Biol 12: 791–798.
11. Shebelut CW, Guberman JM, van Teeffelen S, Yakhnina AA, Gitai Z (2010) *Caulobacter* chromosome segregation is an ordered multistep process. Proc Natl Acad Sci USA 107: 14194–14198.
12. Schofield WB, Lim HC, Jacobs-Wagner C (2010) Cell cycle coordination and regulation of bacterial chromosome segregation dynamics by polarly localized proteins. EMBO J 29: 3068–3081.
13. Leonard TA, Butler PJ, Löwe J (2005) Bacterial chromosome segregation: Structure and DNA binding of the Soj dimer – a conserved biological switch. EMBO J 24: 270–282.
14. Jensen RB, Shapiro L (1999) The *Caulobacter crescentus smc* gene is required for cell cycle progression and chromosome segregation. Proc Natl Acad Sci USA 96: 10661–10666.
15. Mohl DA, Gober JW (1997) Cell cycle-dependent polar localization of chromosome partitioning proteins in *Caulobacter crescentus*. Cell 88: 675–684.
16. Viollier PH, Thanbichler M, McGrath PT, West L, Meewan M, et al. (2004) Rapid and sequential movement of individual chromosomal loci to specific subcellular locations during bacterial DNA replication. Proc Natl Acad Sci USA 101: 9257–9262.
17. Jensen RB (2006) Coordination between chromosome replication, segregation, and cell division in *Caulobacter crescentus*. J Bacteriol 188: 2244–2253.
18. Easter Jr. J, Gober JW (2002) ParB-stimulated nucleotide exchange regulates a switch in functionally distinct ParA activities. Mol Cell 10: 427–434.
19. Ebersbach G, Ringgaard S, Möller-Jensen J, Wang Q, Sherratt DJ, et al. (2006) Regular cellular distribution of plasmids by oscillating and filament-forming ParA ATPase of plasmid pB171. Mol Microbiol 61: 1428–1442.
20. Hill TL (1985) Theoretical problems related to the attachment of microtubules to kinetochores. Proc Natl Acad Sci USA 82: 4404–4408.
21. Peskin CS, Oster GF (1995) Force production by depolymerizing microtubules: Load-velocity curves and run-pause statistics. Biophys J 69: 2268–2276.
22. Raj A, Peskin CS (2006) The inuence of chromosome exibility on chromosome transport during anaphase A. Proc Natl Acad Sci USA 103: 5349–5354.
23. Efremov A, Grishchuk EL, McIntosh JR, Ataullakhanov FI (2007) In search of an optimal ring to couple microtubule depolymerization to processive chromosome motions. Proc Natl Acad Sci USA 104: 19017–19022.
24. Armond JW, Turner MS (2010) Force transduction by the microtubule-bound Dam1 ring. Biophys J 98: 1598–1607.
25. Molodtsov MI, Grishchuk EL, Efremov AK, McIntosh JR, Ataullakhanov FI (2005) Force production by depolymerizing microtubules: A theoretical study. Proc Natl Acad Sci USA 102: 4353–4358.
26. Liu J, Onuchic JN (2006) A driving and coupling "Pac-Man" mechanism for chromosome poleward translocation in anaphase A. Proc Natl Acad Sci USA 103: 18432–18437.
27. McIntosh JR, Grishchuk EL, Morphew MK, Efremov AK, Zhudenkov K, et al. (2008) Fibrils connect microtubule tips with kintetochores: A mechanism to couple tubulin dynamics to chromosome motion. Cell 135: 322–333.
28. Jacob F, Brenner S, Cuzin F (1963) On regulation of DNA replication in bacteria. Cold Spring Harb Symp Quant Biol 28: 329–348.
29. Norris V (1995) Hypothesis: Chromosome separation *Escherichia coli* involves autocatalytic gene expression, transertion and membrane-domain formation. Mol Microbiol 16: 1051–1057.
30. Lemon KP, Grossman AD (1998) Localization of bacterial DNA polymerase: Evidence for a factory model of replication. Science 282: 1516–1519.
31. Hunding A, Ebersbach G, Gerdes K (2003) A mechanism for ParB-dependent waves of ParA, a protein related to DNA segregation during cell division in prokaryotes. J Mol Biol 329: 35–43.
32. Adachi S, Hori K, Hiraga S (2006) Subcellular positioning of F plasmid mediated by dynamic localization of SopA and SopB. J Mol Biol 356: 850–863.
33. Jun S, Mulder B (2006) Entropy-driven spatial organization of highly confined polymers: Lessons for the bacterial chromosome. Proc Natl Acad Sci USA 103: 12388–12393.
34. Doi M, Edwards SF (1986) The theory of polymer dynamics. Oxford: Clarendon Press: 14–16, 22–23, 95.
35. Kramers HA (1940) Brownian motion in a field of force and the diffusion model of chemical reactions. Physica (Utrecht) 7: 284–304.
36. Risken H (1996) The Fokker-Planck quation. Berlin: Springer-Verlag. pp 96–99, 122–125.
37. Anderson JL (1989) Colloid transport by interfacial forces. Annu Rev Fluid Mech 21: 61–99.

38. Golestanian R, Liverpool TB, Ajdari A (2005) Propulsion of a molecular machine by asymmetric distribution of reaction products. Phys Rev Lett 94: 220801.
39. Golestanian R, Liverpool TB, Ajdari A (2007) Designing phoretic micro- and nano-swimmers. New J Phys 9: 126–133.
40. Lee KC, Liu AJ (2008) New proposed mechanism of actin-polymerization-driven motility. Biophys J 95: 4529–4539.
41. Lee KC, Liu AJ (2009) Force-velocity relation for actin-polymerization-driven motility from Brownian dynamics simulations. Biophys J 97: 1295–1304.
42. Sullivan NL, Marquis KA, Rudner DZ (2009) Recruitment of SMC by ParB-parS organizes the origin region and promotes efficient chromosome segregation. Cell 137: 697–707.
43. Campbell CS, Mullins RD (2007) *In vivo* visualization of type II plasmid segregation: Bacterial actin filaments pushing plasmids. J Cell Biol 179: 1059–1066.
44. Pollard TD, Blanchoin L, Mullins RD (2000) Molecular mechanims controlling actin filament dynamics in nonmuscle cells. Annu Rev Biomol Struct 29: 545–576.
45. Cunha S, Woldringh CL, Odijk T (2005) Restricted diffusion of DNA segments within the isolated *Escherichia coli* nucleoid. J Struct Biol 150: 226–232.
46. Elmore S, Müller M, Vischer N, Odijk T, Woldringh CL (2005) Single-particle tracking of *oriC* - GFP uorescent spots during chromosome segregation in escherichia coli. J Struct Biol 151: 275–287.
47. Nicklas RB (1983) Measurements of the force produced by the mitotic spindle in anaphase. J Cell Biol 97: 542–548.
48. Westermann S, Drubin DG, Barnes G (2007) Structures and functions of yeast kinetochore complexes. Annu Rev Biohcem 76: 563–591.
49. Ebersbach G, Gerdes K (2004) Bacterial mitosis: Partitioning protein ParA oscillates in spiralshaped structures and positions plasmids at mid-cell. Mol Microbiol 52: 385–398.
50. Elowitz MB, Surette MG, Wolf PE, Stock JB, Leibler S (1999) Protein mobility in the cytoplasm of *Escherichia coli*. J Bacteriol 181: 197–203.
51. Rapaport DC (1995) The art of molecular dynamics simulations. Cambridge: Cambridge University Press. 251 p.
52. Allen MP, Tildesley DJ (1989) Computer simulation of liquids. Oxford University Press. pp 259–264.